Fuel Processing Technology 212 (2021) 106630

Contents lists available at ScienceDirect

Fuel Processing Technology

journal homepage: www.elsevier.com/locate/fuproc

Research article

Optimizing high-quality graphene nanoflakes production through organic (bio)-precursor plasma decomposition

A. Casanova[a,b], R. Rincón[a,*], J. Muñoz[a], C.O. Ania[b], M.D. Calzada[a]

[a] Laboratory of Innovation in Plasmas (LIPs), Universidad de Córdoba, 14071 Córdoba, Spain
[b] POR2E Group, CEMHTI (UPR 3079), CNRS, Université d'Orléans, 45071 Orléans, France

ARTICLE INFO

Keywords:
Graphene
Plasma
Microwave
Atmospheric pressure
Ethanol
Production rate

ABSTRACT

Atmospheric pressure plasma-based technique for the decomposition of biofuels allows obtaining high-quality graphene powder in one step, without the use of neither metal catalysts nor specific substrates. Despite the numerous advantages of this technology as compared to others, it is necessary to optimize the process to produce high-quality graphene at industrial scale. In this research, the influence of the ethanol flows in the 2.00 to 4.00 g h^{-1} range on the production rate and the quality of graphene has been thoroughly assessed, through a deep characterization of the synthetized material by various techniques. The graphene production rate steadily increased for ethanol flows increasing from 2.00 to 3.40 g h^{-1}, presenting a maximum rate of 1.45 and 1.55 mg min^{-1} for 2.90 and 3.40 g h^{-1}, respectively. Higher ethanol flows lead to a decrease in the production rate, favouring the formation of other carbon-based by-products such as methane and ethylene. High-quality graphene is formed in all plasma conditions, with the lowest number of defects being obtained for an ethanol flow of 2.90 g h^{-1} together with hydrogen and carbon monoxide as main gaseous by-products.

1. Introduction

Since it was first discovered in 2004 [1] and owing to its outstanding mechanical, thermal, electrical and optical properties [2] graphene has been in the spotlight of scientific and technological research. Besides, being a two-dimensional layer made out of sp^2-bonded carbon atoms arranged in a honeycomb structure, graphene is the quintessential building block of every other carbon materials such as fullerenes, nanotubes and graphite [3]. Moreover, it is also the basis for many other carbon materials obtained introducing heteroatoms in the structure of graphene [4]. All these configurational and chemical modifications allow tuning graphene properties to suit particular applications that include composites [5], chemical sensors [6], energy storage [7] or the fabrication of flexible displays [8].

Different methods have been developed for the synthesis of graphene, which can be divided into "top-down" methods – those whose strategy is progressively reducing the size of macroscopic-structure carbon sources – or "bottom-up" – those whose strategy is progressively self-assembling the nanostructure from their constituent atoms or molecular fragments. Among them, liquid phase exfoliation (LPE), chemical vapour deposition (CVD) and reduction of graphene oxide (RGO) have shown their capability to be successfully escalated for meeting industrial requirements while showing different drawbacks. On the one hand, while both LPE and RGO exhibit the largest production rates (> 10 g h^{-1}) [9], the graphene synthesized with these methods has typically a large number of structural defects [10] and contains significant amount of oxygen [11,12]. Hence, the resulting product needs further processing to eliminate the surplus graphene oxide in the case of RGO or separation from the liquid solvent in the case of LPE. On the other hand, CVD allows for the synthesis of large-scale graphene monolayers [13] meeting the standards of high structural quality [14]. However, this method needs the use of specific, high-purity metallic substrates, as well as high temperatures and low pressures as processing conditions. Furthermore, the production rates remain low as compared to those obtained with top-down methods. The combination of CVD with plasma technology in plasma enhanced chemical vapour deposition (PECVD) overcomes the dependence of the synthesis process on high temperatures, while the rest of the drawbacks remain [15,16].

Atmospheric-pressure microwave plasmas have shown their capability to synthesize high-quality graphene from the decomposition of organic precursors in absence of a substrate [17–21]. These plasmas show attractive qualities for the implementation of the graphene synthesis process at industrial level reducing the production costs. For instance, they exhibit high stability and reproducibility within a wide range of operational conditions and can work at atmospheric pressure, avoiding the use of costly pumps. Furthermore, acting on plasma

* Corresponding author.
E-mail address: rrincon@uco.es (R. Rincón).

https://doi.org/10.1016/j.fuproc.2020.106630
Received 29 July 2020; Received in revised form 30 September 2020; Accepted 6 October 2020

operational conditions, the reactions taking place in the discharge can be tailored towards the formation of the desired products. Moreover, these discharges are non-thermal plasmas in which the average kinetic energy of electrons (5000–20,000 K) and heavy particles, *i.e.* atoms, ions and molecules, (1200–5000 K) is larger than those required for decomposing organic compounds. Particularly, the latter temperature can be understood as the gas temperature of the plasma. Since electrons are the particles responsible for absorbing the energy of the electromagnetic field used to sustain the discharge and transferring it *via* elastic and inelastic collisions to the rest of the plasma particles, this difference in temperatures means that the energy supplied to the discharge is not unnecessarily used to heat heavy particles, but to induce physical and chemical reactions for the generation of radicals and excited species that would eventually act as precursors for the graphene formation at the plasma exit [20,21]. Therefore, the energy required to sustain these plasmas is reduced. Besides, at atmospheric pressure, the plasma is a collisional environment in which the large number of free electrons ($> 10^{14}$ electrons per cubic centimetre), colliding with the heavy particles avoids the recombination of species at the plasma exit, limiting the size of by-products [22].

Up to date, few studies have reported the synthesis of graphene in atmospheric-pressure microwave plasmas using ethanol as carbon precursor [17,19–21,23–28]. This alcohol is chosen because it favours the formation of graphene over other hydrocarbons or alcohols [20], and is a renewable eco-friendly precursor that can be obtained by fermentation of starch, sugar and crop wastes, thus contributing to the circular economy strategy. Other precursors, such as methanol, dimethyl ether and isopropanol have been also proposed as an alternative to ethanol to feed microwave plasmas [24], but only dimethyl ether resulted in the production of graphene, while isopropanol yielded only carbon soot and methanol did not produce any solid deposit. In the synthesis process by plasma, the precursor is introduced either in gas or liquid phase in the discharge, habitually sustained in flowing argon and contained in a reactor. As a result, a solid deposit consisting of graphene flakes is formed downstream and collected either from a filter or directly from the walls of the reactor. This process takes place in a single step, without requiring the separation of the product from the substrate or the solvent. Moreover, no additional hazardous chemical is needed, which makes the process more environmentally friendly than LPE and RGO. In the literature, a production rate of 2–6 mg h^{-1} was reported with a microwave plasma torch (MPT) (*ca.* 3.4–6.8 L min^{-1} Ar flow, power 250–1050 W) [17,23,24]. A production rate of 2 mg min^{-1} of graphene was obtained from a wave-driven plasma (MDP) working at 2000 W and sustained with 1.20 L min^{-1} of Ar [18], whereas a production rate of 0.07 mg min^{-1} of mixed multi-layer graphene and multi-wall carbon nanotubes was obtained for a surface wave discharge generated with an Ar flow of 0.75 L min^{-1} working at 200 W [19]. In some other studies production rates of "a few hundred" mg h^{-1} have been reported without providing the actual values [25–28].

Recently, a production rate of 1.33 mg h^{-1} was reported for a TIAGO torch (1 L min^{-1} Ar flow, power 300 W) [21]. TIAGO is a device utilized as microwave power coupler for creating and maintaining the plasma. This device presents some advantages in comparison with those used by other authors. Among them, TIAGO torch has high tolerance to ethanol entrance due to a large power density, which is translated into high electron density and gas temperature values, thus favouring the decomposition of substances. Besides, it is possible to form a compact torch array constituted by various TIAGOs disposed in a single waveguide [29], operating at powers from a few hundred watts up to 2–3 kW per each one. This feature makes this device particularly suitable for its implementation at industrial level.

One of the main challenges of plasma technology is increasing the production rate of graphene to values close to those exhibited by top-down technologies [20] without reducing the material quality. With this purpose, different experimental conditions can be tuned, such as the input power, the carrier gas flow, the design of the plasma reactor, or the amount of graphene precursor. In this study, we focused on evaluating the effect of the latter by thoroughly analyzing the impact of the ethanol flow introduced in the discharge in both the production rate and quality of graphene using a TIAGO torch plasma together with the formation of carbon-based gaseous by-products. The results from this study are of foremost interest prior to proposing this technology at an industrial scale, where the use of an array conformed by several torches would lead to a significant increase the production rate of graphene.

The manuscript is organized as follows. In the section Materials and methods describes the experimental arrangement and techniques for the graphene characterization. In the section Results and Discussion, the operational conditions leading to graphene formation are identified, and the experimental results describing the gaseous and solid by-products obtained from the ethanol decomposition are presented and discussed, together with the selectivity of the process and the quality of the obtained graphene. Finally, the conclusions are given in Section Conclusions.

2. Materials and methods

2.1. Experimental set-up

A schematic drawing of the experimental set up can be observed in Fig. 1. The plasma was created by using a TIAGO device, which has been theoretical described and experimentally characterized in [28,30], respectively. The TIAGO torch discharge is a wave-guide structure comprising waveguide and coaxial elements serving the purpose of wave-mode conversion and impedance matching. The discharge was generated at the end of the tip of a cylindrical hollow metallic rod showing a flame morphology which extends to the atmosphere. In this sense, when the plasma torch operates at open air, the molecules coming from it (mainly nitrogen) interact with the discharge provoking changes in the plasma internal kinetics [30–31]. In order to reduce the contact between plasma and the atmospheric air and avoiding flame instabilities due to possible air streams, a cylindrical reactor was concentrically placed around the metallic rod. In this way, the plasma was surrounded by the reactor-contained air which is progressively evacuated over time by the Ar gas flow. The top outflow in the reactor was opened to evacuate the gases in the reactor and maintaining atmospheric pressure into it. A complete and detailed description of the elements forming the set up can be found in our previous works [32,33].

High purity Ar (99.999%) gas was used to initiate and feed the plasma discharge, with flows ranging from 0.15 to 1.00 L min^{-1} adjusted by a HI-TECH mass flow controller (HI-TECH, Bronkhorst). The discharge was generated at the end of the tip of a cylindrical hollow metallic rod showing a flame morphology. After plasma ignition, 99.5% pure ethanol (EtOH) was introduced in the discharge in gas phase through a steel tube heated at 110 °C to prevent condensation. Ethanol vaporization was carried out in a gas-phase liquid delivery system (CEM, Bronkhorst) able to introduce ethanol flows ranging from 0.20 to 10.00 g h^{-1}.

Microwave powers (200–500 W) were supplied in a continuous mode by a 2.45 GHz SAIREM microwave generator (GMP KG/D) equipped with a water-cooled circulator to avoid power reflection damage. The reflected power was kept below 5% of the input power using a short circuit movable plunger and a triple stub as impedance matching means [30].

A cylindrical glass reactor was concentrically placed around the metallic rod to reduce the contact between the plasma and the atmospheric air, avoiding flame instabilities due to possible air streams. The reactor also acted as chamber for the recovery of the carbonaceous solid (*e.g.* graphene flakes); the plasma occupied the center bottom part of the reactor and as the production of the solid material occurs in the gas phase, it is deposited on the inner wall of the glass reactor. Such graphene flakes are not strongly adhered to the reactor wall, thus the

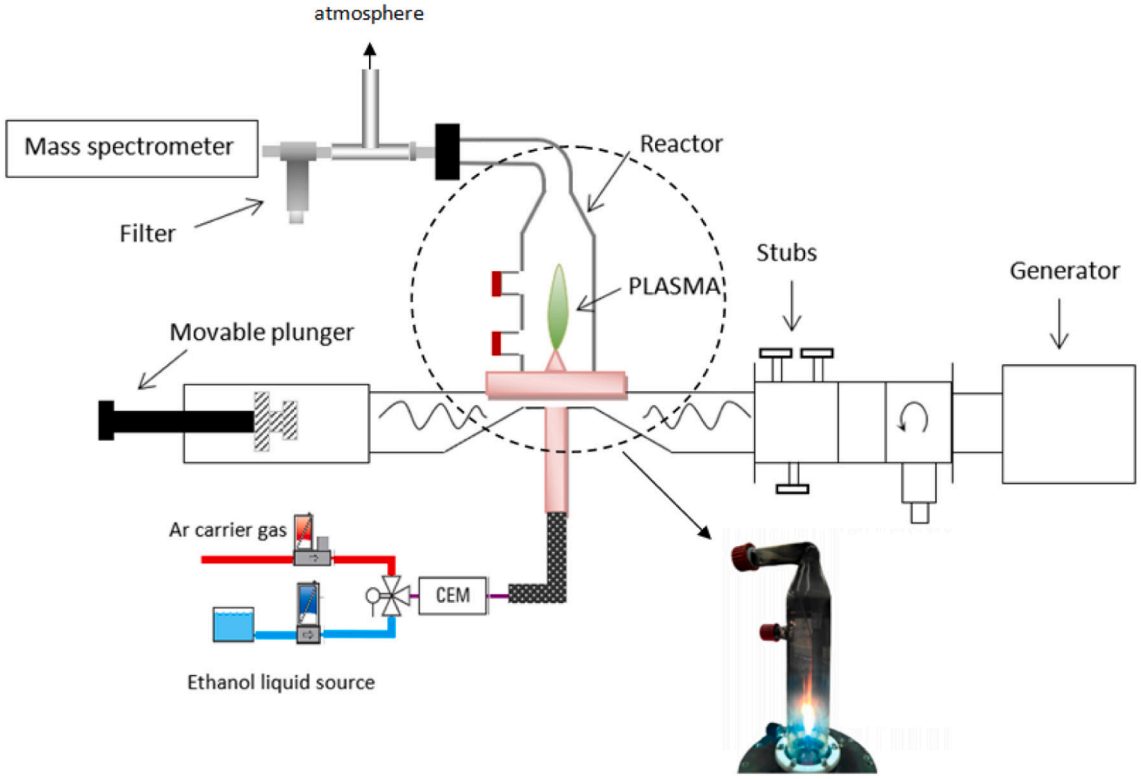

Fig. 1. Schematic drawing of the experimental set up (no to scale).

powders are easily collected by sweeping with a small brush without needing the use of any solvent or other complementary process.

The probe of a quadrupole mass spectrometer (QMS, PTM63 1121, mod. Omnistar, Pfeiffer Vacuum Technology) was coupled to the reactor top out flow with two purposes; one of them to monitor the air (nitrogen) content into the reactor and the other one to analyze the gaseous by-products from the ethanol decomposition. A filter (33127–201, Iberfluid) was placed between the glass reactor and the spectrometer probe to avoid the entrance of solid material into the mass spectrometer and prevent external contamination. The molar production values of gaseous by-products (H_2, CO, C_2H_2, C_2H_4 and CH_4) was obtained upon previous calibration of the mass spectrometer considering the calibration factors and sensitivity coefficient of each gas.

Graphene production rate is calculated as the total amount of graphene powders obtained over a period of time and averaged for two batches. Graphene powders were collected from both the reactor wall and the filter, the latter amount being smaller (less than 25% of the total mass) but of the same quality and characteristics. The synthesis time is exclusively considered as the time where graphene formation occurs, i.e. time in which plasma operates under appropriate conditions for the synthesis of the material.

2.2. Characterization of the solid product

Images of the solid deposit obtained upon plasma decomposition of ethanol were obtained by low-magnification TEM using a JEOL JEM 1400 operated at 120 kV and High-Resolution TEM (HRTEM) with a FEAI Tecnai G2F30 s-Twin microscope (0.2 nm point resolution) operated at 200 kV of accelerating voltage. Powder X-ray diffractograms were recorded in a Bruker D8 Advance diffractometer operating a 40 mA, using CuKα (0.154184 nm) radiation. XRD patterns were collected in the range 5–90° with a 0.06° step size. Solid samples were also characterized by Raman Spectroscopy in the 750–3500 cm-1 range using a Renishaw in *Via* confocal Raman Microscope equipped with a 514 nm and 20 mW NdYAG laser with a spot of 0.8 μm and an acquisition time of 30 s. X-ray photoelectron spectroscopy (XPS) experiments were recorded in a PHOIBOS HSA3500 150 R6 MCD-9 spectrometer, with the solid material placed at the surface of a Mb holder. Survey spectra from zero to 1400 eV and high-resolution spectra (focused on C1s and O1s) were recorded using a standard Al X-ray source. The pass energy was 40 eV with a step of 1 eV for survey and 35 eV with a step of 0.1 eV for high resolution spectra. Processing of the collected spectra (MultiPakTM software) was performed using the C1s peak of adventitious carbon at 284.4 eV as energy reference. A Shirley-type background function and a Gaussian (90%)–Lorentzian (10%) peak shape was utilized for the deconvolution of C1s peak which allows for the identification of bond types in the material samples.

3. Results and discussion

3.1. Operational conditions for the formation of graphene: ethanol decomposition routes

In order to optimize the TIAGO torch to produce mass scale graphene, it is crucial to find the limits and the optimal operational conditions of this microwave plasma device, so as to control the capability of Ar-TIAGO discharges to withstand the introduction of ethanol as graphene precursor. Our previous work [30] demonstrated that TIAGO torch discharges open to the air can operate in a wide range of argon flows (0.15 to 5.00 L min^{-1}) and input powers (200 to 500 W), ensuring plasma stability since the reflected power always remained below 5% of the input power. Hence, power operating conditions were fixed accordingly to explore the capability of the plasma to withstand EtOH introduction as function of argon flow. Moreover, even considering that processes in plasmas typically occur in small timescales, the decomposition of ethanol might require several steps and, consequently, the molecules must remain in contact with the plasma enough time to allow them to take place. Thus, when working with plasmas sustained in a flowing gas, it is important to consider the average time each molecule spends within it, i.e.: the residence time, which depends

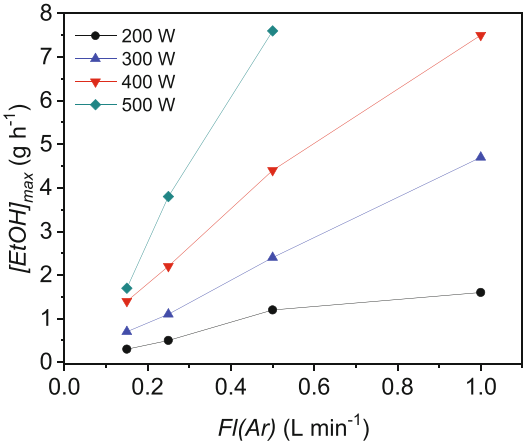

Fig. 2. Maximum ethanol inlet withstood by Ar TIAGO plasmas sustained at different Ar flows and input powers.

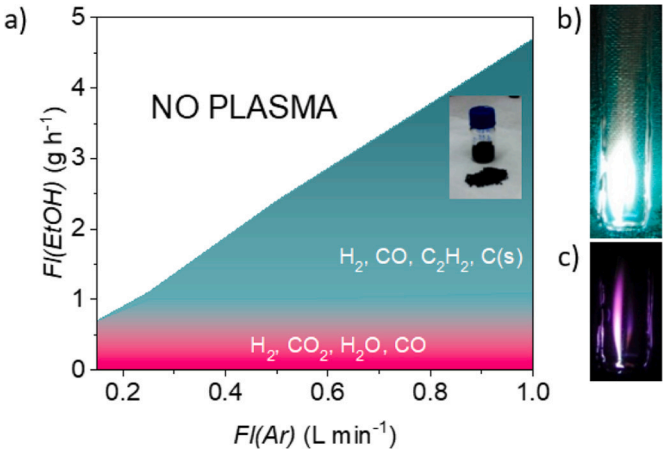

Fig. 3. (a) Schematic representation of products obtained from both fundamental routes for ethanol decomposition in an Ar-TIAGO torch plasma sustained with 300 W and pictures of Ar-EtOH discharges sustained with 1.00 L min^{-1} of argon and (b) 1.00 g h^{-1} and (c) 0.22 g h^{-1} of ethanol.

on the total gas flow among other factors. Therefore, the maximum Ar flow was limited to 1.00 L min^{-1} to avoid short residence times that would lead to a decrease in the solid carbon production rate, as reported in [28,34].

Fig. 2 shows the maximum ethanol flow that can be added to an Ar plasma discharge before its extinction as a function of both the Ar flow and the input power. The extinction of the discharge is a result of an inefficient energy coupling (*e.g.*, reflected power above 5%) between the transmission line and the plasma impedances. For a fixed Ar flow and input power, the ethanol flow was increased while using the matching means to keep the reflected powers below 5% of its input value. When it was no longer possible to properly couple the microwave power, the input power was increased by 100 W. Thus, for a given Ar flow, the discharge cannot be sustained with ethanol amounts higher than those shown in Fig. 2 for each specific power value. Moreover, for a constant input power, the larger the argon flow, the higher the ethanol amount which can be fed to the discharge. This points out that the maximum amount of ethanol to sustain the plasma discharge depends on its dilution rate in the Ar-EtOH mixture, rather than on the absolute amount of ethanol added to the argon flow. Furthermore, as it can be seen, plasmas sustained with higher input powers withstand larger ethanol amounts.

The kinetics of Ar-TIAGO torch plasmas is highly affected by the air environment surrounding the discharge [30], which is a key experimental consideration for the ethanol decomposition pathway. Optical emission spectra of Ar-EtOH discharges have shown that the entrance of air (at low Ar and EtOH flows) in the discharge favours the formation of CN species, but when the air entrance is reduced (by increasing Ar and EtOH flows), C_2 species are formed [31,32]. In this last case, the temperature of the gas is also increased, favouring the decomposition of ethanol into a solid carbon material and H_2 and CO as main gaseous by-products. On the other hand, when low flows of argon or ethanol are used, the decomposition of ethanol only produces gaseous by-products (*e.g.*, H_2, H_2O, CO or CO_2) [31].

These results allowed to identify two routes of ethanol decomposition for plasmas sustained at 300 W with different Ar and EtOH flows as it appears depicted in Fig. 3a. In addition, the dependence of the formation of different plasma species on the argon flow brings about differences in the plasma colour and its external morphology, as it can be observed in Fig. 3b and c, corresponding to the formation of C_2 (emission in the 450–600 nm range) and CN species (violet emission within the 350–400 nm range) linked to low and high air entrance, respectively, which is translated to the nature of by-products obtained at the plasma exit as it has been mentioned above.

In this context, this study was carried out using 1.00 L min^{-1} of argon flow and 300 W of microwave power. The Ar flow was chosen because it is the most suitable value to withstand larger ethanol amounts, favouring solid carbon formation while keeping moderate powers. Besides, these experimental conditions allow the comparison with previously reported results [33]. For these operating conditions, a maximum ethanol flow of 4.40 g h^{-1} can be fed to the plasma, while the formation of solid carbon will only take place for ethanol amounts larger than 0.90 g h^{-1}. Considering this, ethanol amounts between 2.00 and 4.00 g h^{-1} were considered in this investigation.

3.2. Operational conditions for the formation of graphene: ethanol decomposition routes

According to the objective of this work, once the operating conditions of the TIAGO torch plasma regarding input power and argon flow were selected (300 W and 1.00 L min^{-1} of Ar), different amounts of ethanol were added to the discharge (*e.g.*, 2.00, 2.90, 3.40, 3.80, 4.00 g h^{-1}) to determine the influence of this parameter on the formation rate and quality of a solid carbonaceous material. The production rates at each experimental condition are compiled in Table 1. Data correspond to the average production rates of different batches for each condition.

As it can be seen, the solid carbon production presents a gradual increasing pattern with the flow of ethanol up to a value of 3.40 g h^{-1}; from this amount, higher ethanol flows resulted in lower production rates. It is important to remark that these values are not referred or normalized to the organic precursor utilized for the formation of the material which will be evaluated and discussed in forthcoming paragraphs. In a previous study [21] carried out under similar experimental conditions of Ar flow (1 L min^{-1}), EtOH flow (2 g h^{-1}) and input power (300 W), a production rate of 1.33 mg min^{-1} was reported; this difference can be attributed to slight modifications in the geometry of the reactor. The reactor geometry, including dimensions, has been described as an important factor which determines the formation of solid carbon material from the decomposition of a precursor by a plasma

Table 1
Solid carbon production rate.

Fl(EtOH) (g h^{-1})	Production rate (mg min^{-1})
2.00	1.08 ± 0.07
2.90	1.45 ± 0.04
3.40	1.55 ± 0.04
3.80	1.43 ± 0.07
4.00	1.17 ± 0.03

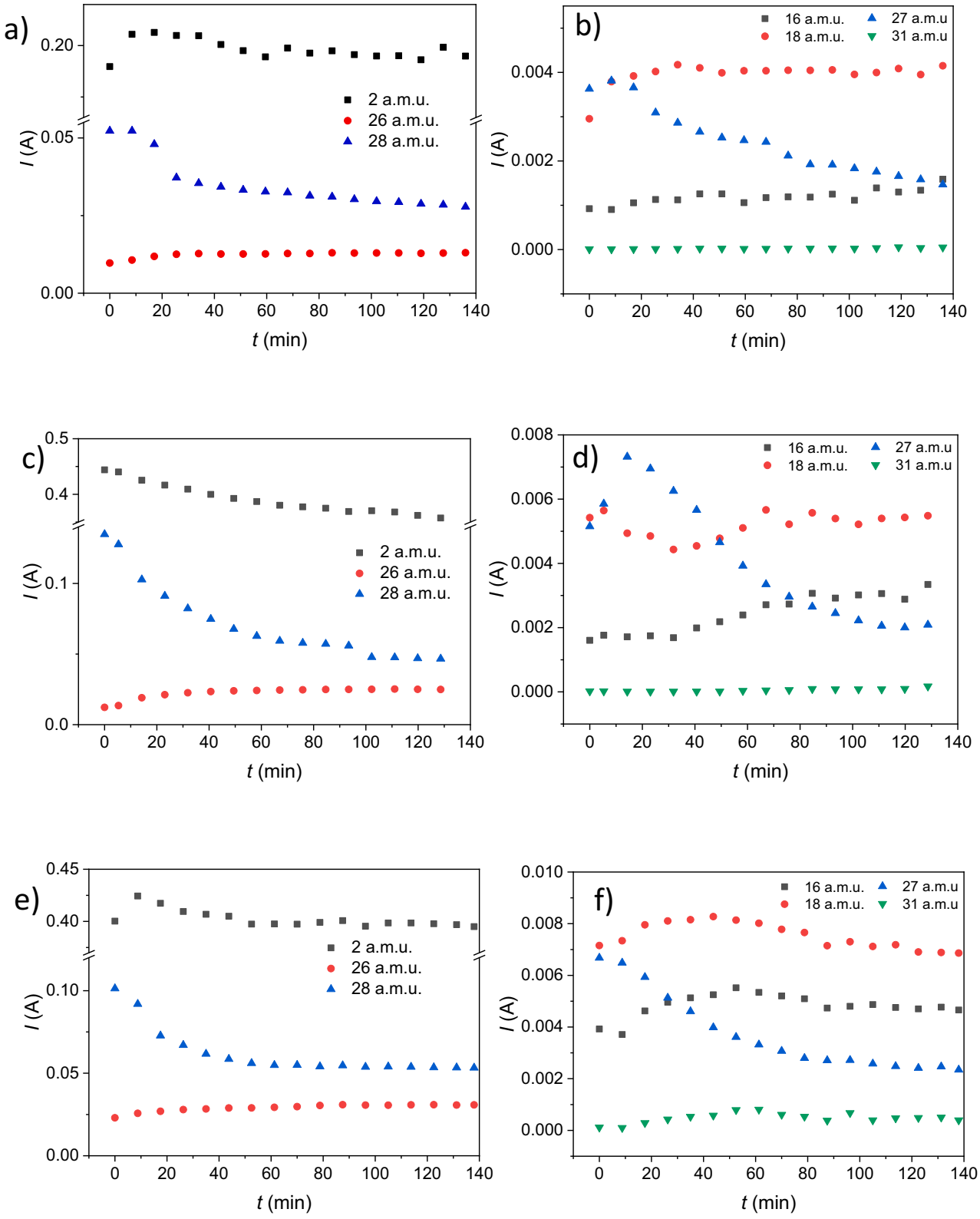

Fig. 4. Ion intensity *versus* time of mass fragments of group 1 (2, 26 and 28 a.m.u.) and group 2 (16, 18, 27 and 31 a.m.u.) for 2.00 (a and b), 3.40 (c and d) and 4.00 (e and f) g h^{-1} of ethanol added to the plasma.

[20].

With the view of optimizing the graphene production and analyzing the long-term stability of the process, a mass spectrometer was coupled at the exit of the reactor to identify and quantify the different gaseous by-products resulting from ethanol decomposition. The gas exhaust stream flow was sampled for on-line gas analysis; mass-to-charge ratios, *m/z*, ranging from 1 to 100 a.m.u. were recorded. It should be noted that no signals for gaseous products over *m/z* 85 a.m.u. were detected in any mass spectrum; this is expected since plasmas at atmospheric pressure yield small and simple molecules due to the great number of

collisions between electrons and plasma heavy particles [22]. Besides, the detection of low signals at m/z 50 and 78 a.m.u may suggest the almost negligible formation of diacetylene and benzene or 2,4-hexadiyne, respectively [34]. Thus, only the signals up to m/z 45 a.m.u were considered for the identification of the gaseous products.

Fig. 4 shows the evolution of the ion current intensity of different mass fragments related to ethanol decomposition and gas formation for 2.00, 3.40 and 4.00 g h^{-1} of ethanol fed to the plasma. These ethanol conditions represent the extreme ethanol values considered (*i.e.*, 2.00 and 4.00 g h^{-1}), while 3.40 g h^{-1} of ethanol yields the maximum production of solid carbon (Table 1). It is worth mentioning that even though the experiment time was not necessarily the same in all the experimental conditions, the behaviour of ion current intensities with time is similar. The detailed analysis of the temporal behaviour of the detected gaseous products depicted in Fig. 4 can be carried out considering two groups: group 1 for *m/z* equal to 2, 26 and28 a.m.u (Fig. 4a, c and e) and group 2 for m/z equal to 16, 18, 27 and 31 a.m.u (Fig. 4b, d and f). It can be observed that the only signals showing a significant variation are those corresponding to mass fragments 28 (Fig. 4a, c and e) and 27 a.m.u. (Fig. 4b,d and f). These signals stabilize after ~60 min in all cases, suggesting that these fragments can be attributed to a gas whose concentration decreases over time (*e.g.*, air evacuated from the reactor) and does not participate in the decomposition of ethanol at long reaction times. Furthermore, from Fig. 4 it can be derived the behaviour of ion currents with the time, for all signals, is the same, not depending on the ethanol added to the plasma. In addition, note that the formation of the solid material starts when the air has been evacuated from the chamber; i.e., graphene formation time and experiment time are not the same.

The identification of the gaseous by-products through the *m/z* signal intensities was performed using the theoretical mass spectra given by NIST Library from Varian MS Workstation (version 6.6) based on the relative intensity of mass fragments (base and secondary peaks) related to electron-impact mass spectra of possible species [35]. Fig. 5 shows the mass spectra of the Ar-EtOH plasmas for the experimental conditions considered in Fig. 4 after 140 min of ethanol decomposition reaction and once the formation of the gas by-products in the reactor was stabilized after the evacuation of the air inside the plasma reactor. Spectra corresponding to Ar plasma without ethanol is also shown for comparison. Unfortunately, pure argon plasmas are unstable without the existence of a non-ionized gas [36], i.e. air, therefore, note that air is present when analyzing pure Ar plasma mass spectra. Ion current intensities were normalized to $m/z = 40$ a.m.u signal, which was the maximum one corresponding to Ar^+. Other peaks at *m/z* 20 (Ar^{++}), 36 and 38 (Ar isotopes) together relevant mass fragments related to air surrounding the discharge (e.g 14, 15, 16, 18, 26, 28 and 32) were detected.

Concerning the identification of gaseous by-products during ethanol decomposition after the evacuation of air, the $m/z = 31$ a.m.u signal (hydromethyl cation, $^+CH_2OH$) was used to control ethanol decomposition rate by the plasma (detail in Fig. 5), allowing us to determine a conversion rate higher than 98% for all the ethanol flows, calculated as described in Eq. (3) of reference [33]. When the air is removed from the plasma chamber, i.e. experiment times longer than 60 min, it can be assumed that (i) *m/z* equal to 28 can be certainly attributed to CO and/or C_2H_4 and (ii) the formation of HCN (m/z 27 u.m.a.) can be completely discarded. According to Fig. 5, C_2H_5OH is mainly transformed into molecular hydrogen (H_2, m/z = 2 a.m.u.) and carbon monoxide (CO, m/z = 28 a.m.u.). Both carbon monoxide and ethylene (C_2H_4) can contribute to m/z = 28 a.m.u. In fact, the presence of mass 27 suggests the existence of ethylene, whose contribution has been subtracted from the intensity of mass 28 to determine the intensity corresponding to CO. The low contribution of ethylene to m/z = 28 a.m.u. suggests that it is formed at trace level. In addition, the intensity ratio of m/z 26/25/24 follows the typical 100/25/5 ratio of acetylene (C_2H_2), thus implying the formation of this gas. The formation of methane (CH_4) and water

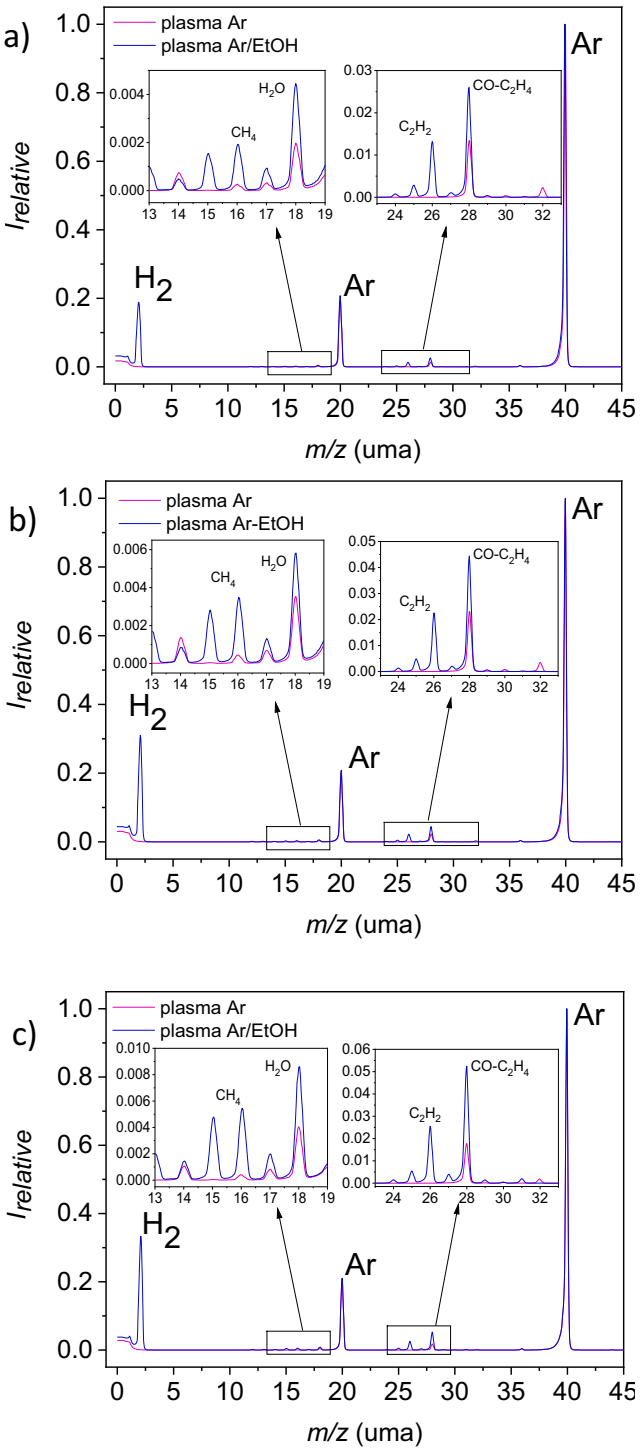

Fig. 5. Comparison of mass spectra of gases from pure Ar plasma (in air atmosphere) and Ar-EtOH (2.00, 3.40 and 4.00 g h^{-1}) plasma after gaseous by-products stabilization (60 min).

(H_2O) can be verified from the relative intensities of m/z 16 and 15 a.m.u., and m/z 18 and 17 a.m.u., respectively. The formation of H_2, CO, C_2H_2, C_2H_4, CH_4, H_2O and solid carbon upon decomposition of ethanol by a TIAGO torch plasma is in agreement with the theoretical study carried out by Tsyganov et al. about the decomposition of ethanol by a microwave plasma [28].

The amount of solid carbon formed decreased at high ethanol flows (> 3.40 g h^{-1}), despite the higher amount of carbon precursor (Table 1). To understand this behaviour, the molar production rate

Table 2
Molar production rate of CO, C_2H_2, CH_4, C_2H_4 and C(s) as function of the flow of the reactant.

Fl(EtOH) (g h^{-1})	Molar production ($\cdot 10^{-2}$ mmol min^{-1})				
	CO	C_2H_2	CH_4	C_2H_4	C(s)
2.00	68.4 ± 0.2	26.6 ± 0.1	2.53 ± 0.02	3.1 ± 08	8.9 ± 0.6
2.90	104.4 ± 0.4	39.4 ± 0.2	2.35 ± 0.05	6.6 ± 0.2	12.1 ± 0.4
3.40	120.2 ± 0.6	48.8 ± 0.3	5.52 ± 0.08	8.5 ± 0.6	12.9 ± 0.4
3.80	132.4 ± 0.6	53.2 ± 0.4	8.28 ± 0.02	11.3 ± 0.2	11.9 ± 0.6
4.00	130.5 ± 0.6	59.2 ± 0.5	11.28 ± 0.05	12.6 ± 0.2	9.8 ± 0.2

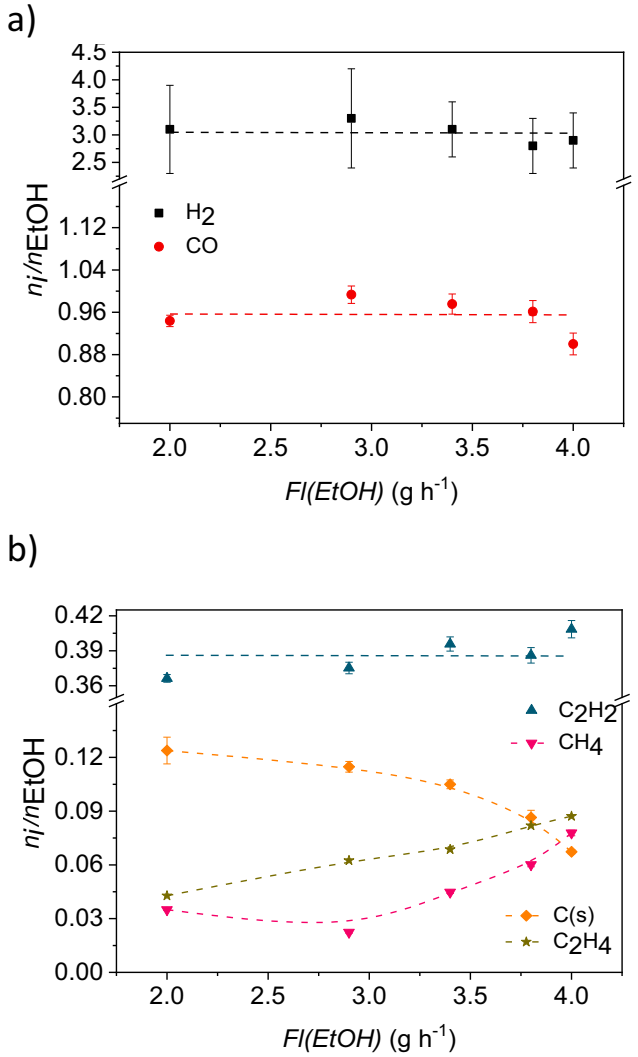

Fig. 6. Mol formation of (a) H_2, CO, (b) C_2H_2, CH_4, C(s) and C_2H_4 per mol of ethanol feed to the discharge.

(mmol min^{-1}) of each carbon-based compound (*i.e.*, CO, C_2H_2, CH_4 and C_2H_4) was calculated and shown in Table 2. It is worth mentioning that the molar production rate could be calculated from ion intensities of the mass fragments by knowing Mass Spectrometer calibration factors of each compound. Unlike the trend observed for solid carbon, the molar production of CO, C_2H_2, CH_4 and C_2H_4 increased with ethanol flow. The trend is more pronounced for CO and C_2H_2, especially at higher ethanol flows. Since higher amounts of ethanol fed to the discharge promote higher number of C atoms available in the discharge, the molar production of carbon-based by-products as well as H_2 per molar flow rate of ethanol were evaluated (Fig. 6). As it can be seen, the amount of H_2, CO and C_2H_2 produced per molar flow rate of ethanol was rather similar for all the ethanol flows. Nevertheless, small but significant variations were observed in the production of CH_4, C_2H_4 and solid carbon; the higher amounts of the gases formed for the largest flows of ethanol are accompanied by a low production of solid carbon. These results agree with those reported by Jiménez et al. [34], who found the formation of high amounts of methane linked to a lower production of solid carbon. Besides, the influence of the production of high amounts of hydrogen from ethanol decomposition on the yield of solid carbon formation cannot be discarded since, as it was shown by Tsyganov et al. [28] when additional hydrogen is present, the total solid carbon yield decreases.

In order to show the relative importance of the minor gases (*i.e.*, C_2H_4 and CH_4) in the composition of the by-products, Fig. 7 shows a comparison between the correlation of the number of carbon atoms in the reactant introduced in the plasma (ethanol) and those in the carbon by-products. The two situations compared correspond to the case when C_2H_4 and CH_4 are not accounted for and *vice versa*. As it can be seen, the number of carbon atoms in ethanol correlates well with the sum of the carbon atoms obtained when the contribution of all carbon-based by-products (CO, C_2H_2, CH_4, C(s) and C_2H_4) is considered. Interestingly, when only the contribution of CO, C_2H_2 and C(s) is taken into account, the mismatch in the calculation is more noticeable at larger ethanol flows. This highlights that large EtOH flows favours the formation of CH_4 and C_2H_4 over C(s) which might be partially due to a higher H_2 production under this condition as it is pointed out in [28] or changes in plasma internal parameters (e.g.: gas temperature, electron density…) [34]. This finding is remarkable, since it demonstrates that the modification of the operational conditions of Ar-EtOH TIAGO torch discharge, in particular, the amount of ethanol added to the plasma gas can also direct the decomposition of ethanol towards a preferential formation of either gaseous or solid by-products.

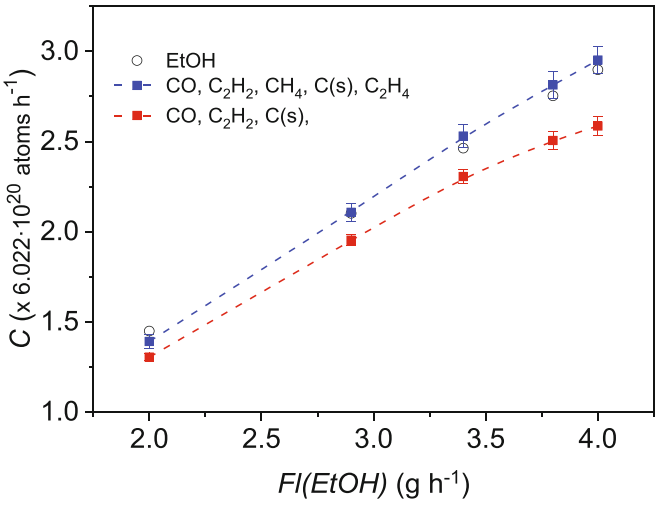

Fig. 7. Content of atomic carbon flow in the reactant (EtOH) and in carbon-based by-products considering two situations: ■ CO, C_2H_2, CH_4, C(s) and C_2H_4) and ■ CO, C_2H_2 and C(s).

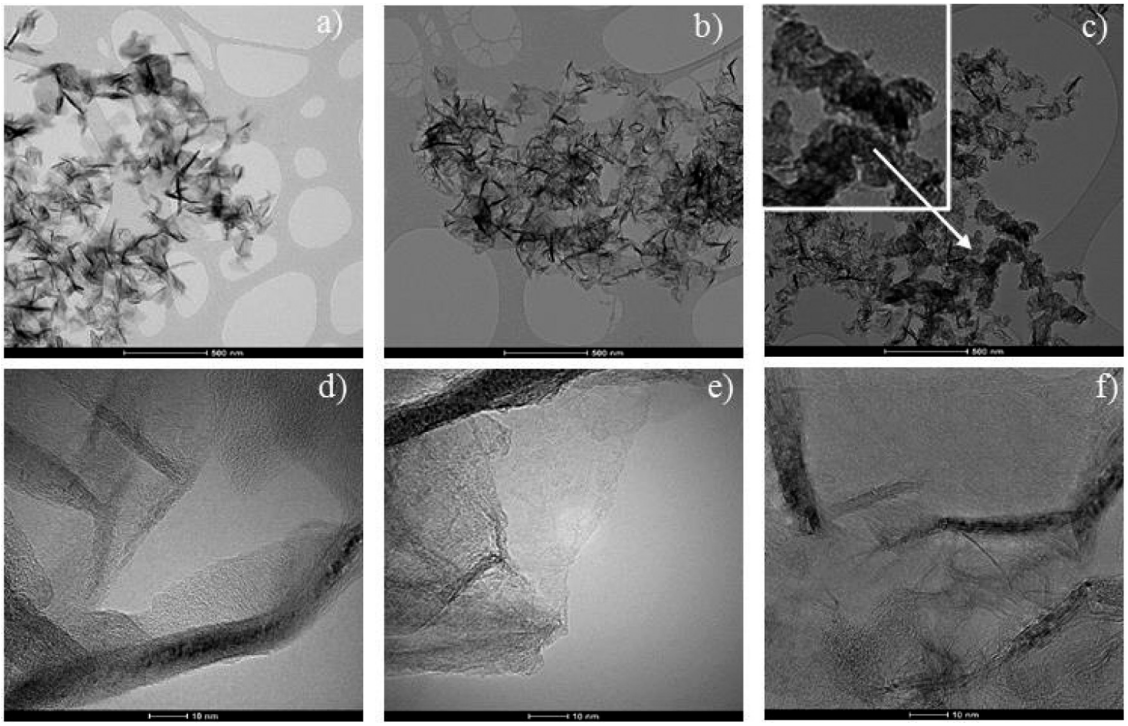

Fig. 8. (a, b, c) TEM and (d, e, f) HRTEM images of the material obtained by the decomposition of (a, d) 2.00 g h^{-1}, (b, e) 3.40 g h^{-1} and (c,f) 4.00 g h^{-1} of ethanol.

3.3. Graphene as by-product at the plasma exit

The solid carbon synthesized has been characterized by the techniques described in Section Materials and methods. Fig. 8a, b and c shows low-magnification TEM images of the material obtained from the decomposition of 2.00, 3.40 and 4.00 g h^{-1} of ethanol.

The characteristic structure of graphene sheets can be identified in all TEM images, *e.g.* areas with high transparency which is related to only few graphene layers [21]. Dark zones can be ascribed to folded graphene sheets. It must be noted that some carbonaceous particles can be only identified in the material obtained for the case of 4.00 g h^{-1} of EtOH. Representative high-resolution TEM images of samples obtained in the aforementioned ethanol conditions (Fig. 8d, 8e and 8 f) show graphene sheets with different number of layers as well as curved graphene sheets, *i.e.* tortuous graphene layers which are framed in the pictures. Similar images were found for the materials obtained under the rest of experimental conditions. It should be noted that even though plasma decomposition of ethanol leads to the formation of carbon deposits, their morphology and structure highly depends on the operating system and conditions; for instance, the formation of either nanotubes/graphene composites [19] or graphene [21] depends on the plasma source, the existence or absence of contact with the air surrounding the discharge, *etc.* In this regard, further characterization of the carbon deposits by XRD and Raman spectroscopy confirmed the production of graphene. XRD diffractograms of the samples are shown in Fig. 9. Regardless of the experimental conditions, all the patterns present a strong diffraction peak at 2θ~26.0° which corresponds to the (002) plane of graphitic materials, along with weaker peaks at 2θ~42.7° and 2θ~44.0° corresponding to (100) and (101) planes, respectively. The position of the strongest diffraction peak at 2θ~26.0° is slightly downshifted as compared to graphite [37], indicating higher interlayer distances in the structure. The interlayer spacing for the (002) plane was 0.3437 ± 0.0010 nm, which is characteristic of graphenic materials [38,39].

Raman spectra of the obtained samples is shown in Fig. 10, observing the presence of G, D and 2D bands. The analysis of the positions of these bands gives information about the structural characteristics of the

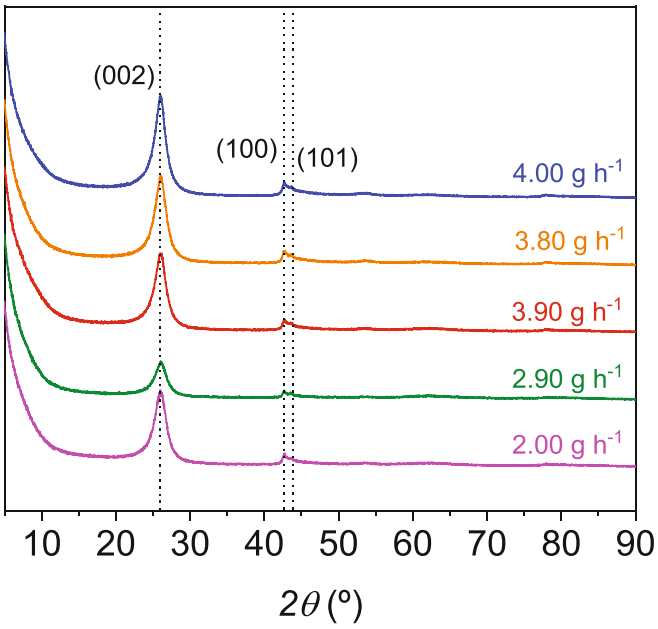

Fig. 9. XRD diffraction patterns of samples synthetized by plasma processing with different ethanol flow.

materials. The G (~ 1580 cm^{-1}) and 2D (~ 2700 cm^{-1}) bands, characteristic of graphene, were observed in all the samples regardless the flow of ethanol, demonstrating the synthesis of this material through the process used in the current investigation [40]. The D band (~1350 cm^{-1}) associated with defects in the graphene [41], can be also seen in the Raman spectra. The position of the G band confirms that the presence of graphene oxide can be discarded because it is located at ~ 1594 cm^{-1} [42,43]. The relative intensities of these bands (I_D/I_G and I_{2D}/I_G) are also commonly used to provide information about the quality and to quantify defects present in graphenic materials. As it is observed in the spectra, the intensity of the D band is much lower than

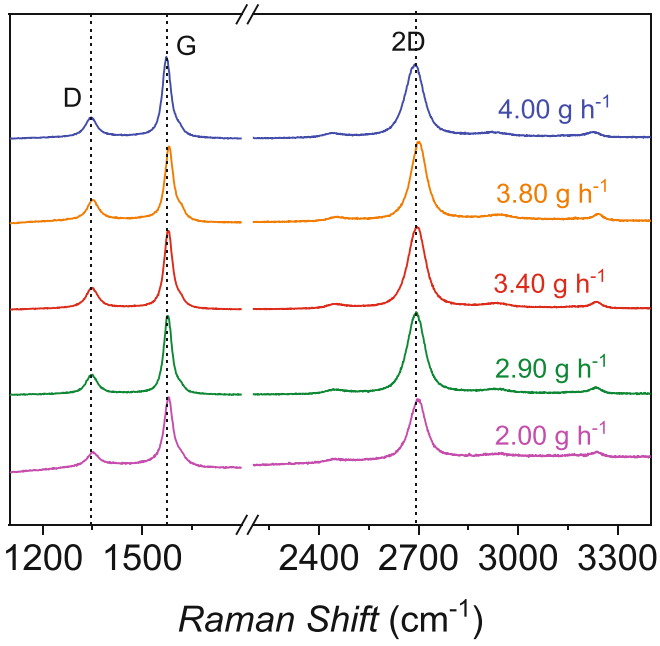

Fig. 10. Raman spectrum of samples synthetized through the plasmas process described in the current research.

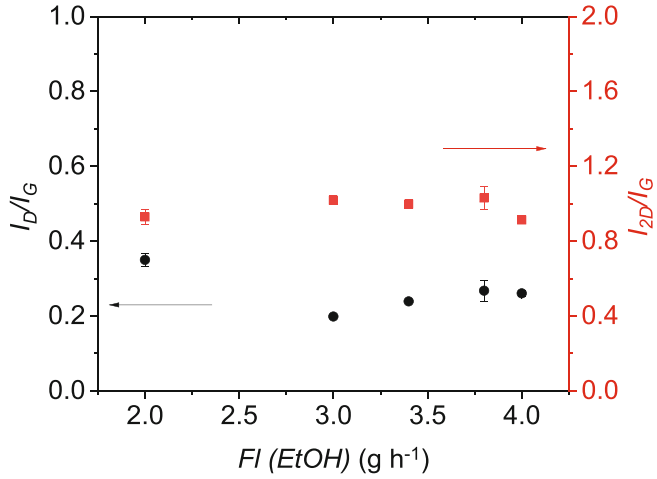

Fig. 11. I_D/I_G (black circles) and I_{2D}/I_G (red squares) values for the samples obtained by the decomposition of different ethanol amounts. (For interpretation of the references to colour in this figure legend, the reader is referred to the web version of this article.)

that of G band, indicating a low number of defects in the synthesized materials. The I_D/I_G and I_{2D}/I_G ratios are depicted in Fig. 11. Values of I_D/I_G range between 0.20 and 0.35, corroborating the low number of defects. According to literature, the shape and position of 2D band can provide information about the number of layers [44–51]. If the 2D peak is characterized by a very sharp, symmetric, and Lorentzian profile with an intensity greater than twice the G peak, the material is constituted by single-layer graphene. In contrast, if the 2D band is wider and its profile can be resolved into two or more components, the sheets are formed by few layers [52]. Due to the difficulty to obtain a reliable deconvolution of the 2D band, the I_{2D}/I_G value can also be used for this purpose; as the number of layers increases, this ratio tends to be lower than 2. Fig. 11 shows that for our materials, I_{2D}/I_G value tends to be constant and equal to the unity, which is associated to few-layer graphene. Only in the case 4.00 g h^{-1} of ethanol, the I_{2D}/I_G value is slightly lower than 1, pointing out to an increase in the number of graphene layers, as also observed in Fig. 8 f.

Table 3
Crystalline domain size (L_a) of graphene sheets obtained through ethanol decomposition.

Fl(EtOH) (g h^{-1})	L_a (nm)
2.00	6.98
2.90	11.57
3.40	10.23
3.80	8.00
4.00	7.09

Other structural parameters characterizing graphene sheets can be derived from Raman spectra, such as the crystalline domain size, L_a (average in-plane length). This parameter was calculated by (1) as suggested by Larouche and Stanfield [53] for tortuous graphene samples, as observed in the TEM images for our materials (Fig. 8). The values are compiled in Table 3.

$$L_a = 4.4\left(\frac{A_D}{A_G}\right)^{-1} \text{nm} \quad (1)$$

This expression is similar to that given by Knight and White [54] by using the ratio of the integrated areas of the D and G bands, A_D and A_G, respectively. The L_a value from (1) is a measure of the small planar graphene units that constitute graphene layers. The higher values of L_a correspond to samples obtained by plasma sustained with ethanol flows of 2.90 and 3.40 g h^{-1}. These L_a values are similar to those reported for few layers graphene synthetized by CVD [55], confirming the high quality of the graphene obtained by plasma decomposition of ethanol under our experimental conditions.

The surface composition of the material was analyzed by XPS. Fig. 12 shows data corresponding to the material synthesized with 3.40 g h^{-1} of ethanol, as a representative example of the different ethanol flows considered.

The survey spectra show that carbon is the majority element (Fig. 12 a), with an oxygen peak (O1s) remarkably less intense than the C1s one at around 400 eV, and a small signal attributed to N1s. The abundance of N1s in the sample always remains below 0.5% regardless of the material analyzed, thus it has been neglected in the discussion. The presence of both oxygen and nitrogen low signals can be attributed to the exposure to the atmospheric air after the material synthesis and thus contamination. This low oxygen-content result rules out the formation of graphene oxide as it was also pointed out by Raman analysis. The C1s peak was deconvoluted into seven functions (Fig. 12b) located at 284.4 eV (sp^2 carbon), 285.5 eV (sp^3 carbon), 286.0 (C—OH), 286.2 (C—O—C), 287.5 eV (C—O), 288.5 eV (COOH) and 290.5 eV ($\pi - \pi^*$). Oxygen-related components are also found through the deconvolution of O1s peak (not shown) for all experimental conditions. The intensity of the peak assigned to sp^3 carbon was significantly lower than that of sp^2 for all conditions. This is in agreement with the low values of I_D/I_G obtained from the Raman spectra, pointing out to a low number of defects in the synthesized graphenes (Fig. 11). Besides, for the peaks corresponding to different groups with oxygen content, their intensities are significantly lower than the signal corresponding to carbon atoms. The high quality of the graphene synthesized in this work is corroborated by the presence of the shake-up satellite peak $\pi - \pi^*$ in the XPS spectra for all conditions [45,55], and also evidences the presence of conjugated aromatic domains.

Fig. 13a shows the correlation between the flow of ethanol and the contributions of sp^2 and sp^3 carbon as detected by XPS. The lowest sp^2 contributions were found for the samples obtained using ethanol flows of 2.00 and 4.00 g h^{-1}. Both samples also displayed the highest contribution of sp^3 sites to C1s. Besides, according to Fig. 13b, both samples exhibit the highest oxygen content (*i.e.* lowest C/O ratio) whereas samples obtained from the decomposition of 2.90 and 3.4 g h^{-1} of

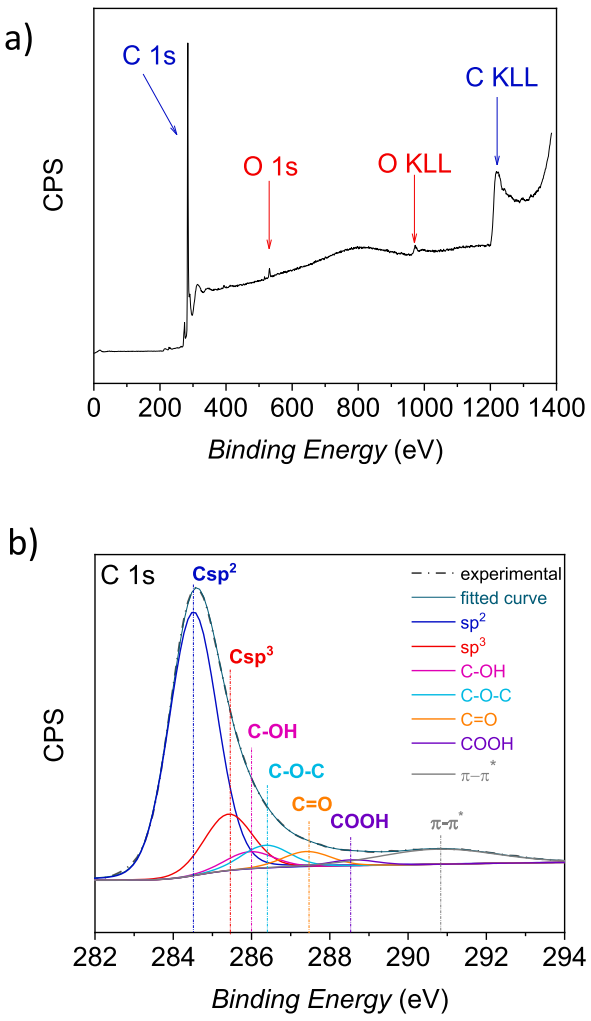

Fig. 12. (a) Survey XPS spectrum, (b) C1s core level XPS spectrum of graphene obtained by the decomposition of 3.40 g h^{-1}.

ethanol exhibit the highest sp^2 contribution.

The results derived from Fig. 13 are in in agreement with the high I_D/I_G and the large L_a values obtained by Raman spectroscopy, indicating the highest quality graphene is obtained with 2.90 and 3.40 g h^{-1} ethanol flows. Interestingly, according to Fig. 13b, oxygen bonds concentration tends to be constant for all the samples with the exception of C-OH and C-O-C bonds, the latter increase with ethanol flow which might suggest different processes taking place inside the reactor during graphene-synthesis.

3.4. Graphene synthesis process: production rate, energy yield and selectivity

To assess the capability of TIAGO torch discharges for large scale production of high-quality graphene, the production rate (mg of graphene per minute, mg min^{-1}) and the energy yield (graphene production rate per applied energy, mg min^{-1} W^{-1}) were calculated and compared with the results reported in the literature for microwave discharges. To that end, graphene selectivity (G^{sel}) was estimated as Eq. (2), being (G^{exp}) the experimental amount of graphene and G^{max-th} the maximum theoretical graphene production; this last one calculated by considering that the most favourable reaction to maximize graphene production would be Eq. (3), where only two carbon-based byproducts are formed from the decomposition of ethanol: graphene (C(s)) and CO.

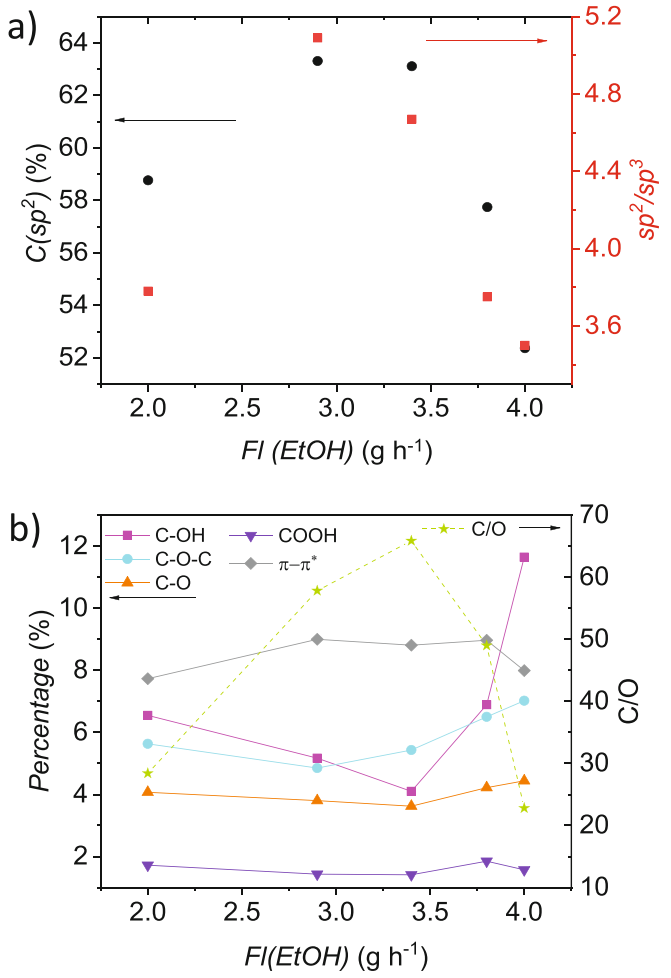

Fig. 13. (a) sp^2 content (black circles) and its ratio between sp^3 content (red squares) *versus* inlet ethanol flow and (b) Percentage of radicals on graphene surface obtained from the deconvoluted C 1 s peak and C/O ratio as function of ethanol flow. (For interpretation of the references to colour in this figure legend, the reader is referred to the web version of this article.)

$$G^{sel} = \frac{G^{exp}}{G^{max-th}} \cdot 100\% \quad (2)$$

$$C_2H_5OH \rightarrow 3H_2 + CO + C(s) \quad (3)$$

According to our results, graphene synthesized by the decomposition of 2.90 g h^{-1} of ethanol shows the highest quality (low number of defects) while the production rate was similar to that found for an ethanol flow of 3.40 g h^{-1}, which showed the maximum value (*ca.* 1.55 mg min^{-1}). So, we have used the results from 2.90 g h^{-1} for comparing the graphene production rates reported in the literature using other microwave devices and ethanol as precursor. Table 4 shows the graphene production rates and energy yields obtained in this work and those reported by other authors. As it can be seen, the highest graphene production rate was obtained by a microwave plasma torch (MPT) working with a high input power, although resulting in a graphene energy yield lower than that obtained working with moderate powers [20,23,24]. Furthermore, it is important to highlight that those values of graphene production were obtained by the decomposition of a large ethanol amount fed to the discharge, which results in low graphene selectivity. From the information presented in the table, TIAGO torch can be pointed out as a promising microwave plasma source for the large scale production of graphene; its graphene production rate and energy yields can compete with the highest values exhibited by a MPT when smaller amounts of EtOH are introduced, being the

Table 4
Comparison of graphene production rate and energy yield using different microwave devices and ethanol as carbon enriched source. The selectivity of the process is also included.

Device	Ethanol flow (mg min^{-1})	Input Power (W)	Production rate (mg min^{-1})	Energy yield (mg min^{-1} W^{-1})	G^{sel} (%)	Ref.
MPT	328	250	2	$8{\cdot}10^{-3}$	2.3	20, 23
MPT	328	1050	6	$5.7{\cdot}10^{-3}$	7.0	24
MDP	–	2000	2	$1{\cdot}10^{-3}$	–	18
SWD	3.7	200	0.07	$3.5{\cdot}10^{-4}$	7.3	19
TIAGO[a]	33.3	300	1.33	$4.4{\cdot}10^{-3}$	15.3	21
TIAGO	48.3	300	1.45	$4.8{\cdot}10^{-3}$	11.5	This work

[a] Reactor design is different from this work.

selectivity of the decomposition of EtOH by a TIAGO torch discharge higher than the obtained by other microwave sources.

4. Conclusions

TIAGO torch microwave discharges working at atmospheric pressure have demonstrated their ability to produce high-quality graphene powders by the decomposition of ethanol as carbon source. An in-depth study of the influence of the ethanol flow on this bottom-up synthesis technique has been carried out paying attention to both the robustness of the system for increasing the flow of ethanol feed to the discharge, and the quality of the synthesized material. This allowed for an optimization of the experimental conditions for maximizing both the amount and the quality of the synthesized graphene.

The capability of an argon-based TIAGO torch plasma to withstand the introduction of various ethanol flows has been assessed. The results show that discharges sustained with this microwave source can steadily operate with ethanol flows as high as 7.60 g h^{-1} considering different argon flows and input powers. However, since the discharge is open to the air, nitrogen and oxygen from the surrounding atmosphere highly affect the kinetics of ethanol decomposition. Thus, the optimized conditions to favour the decomposition of ethanol into solid carbon over other by-products, are 1 L min^{-1} of Ar and 300 W of input power. Under these experimental conditions, the plasma was able to withstand ethanol flows of up to 4.00 g h^{-1}.

Increasing the flow of ethanol resulted in a steady increase of the graphene production rates from 2.00 up to 3.40 g h^{-1} with maximum rates of 1.43 and 1.55 mg h^{-1} for ethanol flows of 2.90 and 3.40 g h^{-1}, respectively, and decreasing the rate for higher flows. According to the analysis of the gaseous by-products, increasing the amount of ethanol favours the formation of methane and ethylene, thus resulting in a lower graphene production rate. In all the experimental conditions considered, high-quality graphene was formed, as evidenced by a high transparency in TEM images, and a low number of defects as extracted from Raman and XPS results. Considering the most promising experimental condition of ethanol flow (2.90 g h^{-1}) in terms of graphene quality, it has been shown that TIAGO torch plasmas exhibit one of the highest graphene energy yield and graphene selectivity among other microwave plasma sources, which certainly points out the high potential of this plasma source for the synthesis of high-quality graphene.

Declaration of Competing Interest

The authors declare that they have no known competing financial interests or personal relationships that could have appeared to influence the work reported in this paper.

Acknowledgements

The authors of the present work are greatly thankful to Prof Michel Moisan, head of the Groupe de Physique des Plasmas (University of Montreal), for the TIAGO torch donation within framework of their active collaboration. This research would not have been possible without this contribution.

This work was partly supported by the XXII-XXIII Programa Propio de Fomento de la Investigación de la Universidad de Córdoba (Spain) (MOD 4.1 PP2017-2018), Project R&D of Spanish Ministry of Science, Innovation and Universities (PID2019-107489GB-I00) and the European Council Research through a Consolidator Grant (ERC-CoG-648161-PHOROSOL).

References

[1] K.S. Novoselov, A.K. Geim, S.V. Morozov, D. Jiang, Y. Zhang, S.V. Dubonos, I.V. Grigorieva, A.A. Firsov, Electric field effect in atomically thin carbon films, Science 306 (2004) 666–669, https://doi.org/10.1126/science.1102896.
[2] G. Mittal, V. Dhand, K.Y. Rhee, S.-J. Park, W.-R. Lee, A review on carbon nanotubes and graphene as fillers in reinforced polymer nanocomposites, J. Ind. Eng. Chem. 21 (2015) 11–25, https://doi.org/10.1016/j.jiec.2014.03.022.
[3] A.K. Geim, K.S. Novoselov, The rise of graphene, Nat. Mater. 6 (2007) 183–191, https://doi.org/10.1038/nmat1849.
[4] H. Lee, P. Keewook, S. Kim, A review of doping modulation in graphene, Synth. Met. 244 (2018) 36–47, https://doi.org/10.1016/j.synthmet.2018.07.001.
[5] X. Sun, H. Sun, H. Li, H. Peng, Developing polymer composite materials: carbon nanotubes or graphene? Adv. Mater. 25 (2013) 5153–5176, https://doi.org/10.1002/adma.201301926.
[6] V. Dua, S.P. Surwade, S. Ammu, S.R. Agnihotra, S. Jain, K.E. Roberts, S. Park, R.S. Ruoff, S.K. Manohar, All organic vapor sensor using inkjet-printed reduced graphene oxide, Angew. Chem. Int. Ed. Engl. 49 (2010) 2154–2157, https://doi.org/10.1002/anie.200905089.
[7] X. Li, L. Zhi, Graphene hybridization for energy storage applications, Chem. Soc. Rev. 47 (2018) 3189–3216, https://doi.org/10.1039/C7CS00871F.
[8] F. Torrisi, T. Hasan, W. Wu, Z. Sun, A. Lombardo, T.S. Kulmala, G.W. Hsieh, S. Jung, F. Bonaccorso, P.J. Paul, D. Chu, A.C. Ferrari, Inkjet-printed graphene electronics, ACS Nano 6 (2012) 2992–3006, https://doi.org/10.1021/nn2044609.
[9] S. Abdolhosseinzadeh, H. Asgharzadeh, H.S. Kim, Fast and fully-scalable synthesis of reduced graphene oxide, Sci. Rep. 5 (2015) 10160, https://doi.org/10.1038/srep10160.
[10] C. Gomez-Navarro, J.C. Meyer, R.S. Sundaram, A. Chuvilin, S. Kurasch, M. Burghard, K. Kern, U. Kaiser, Atomic structure of reduced graphene oxide, Nano Lett. 10 (2010) 1144–1148, https://doi.org/10.1021/nl9031617.
[11] L. Dong, Z. Chen, X. Zhao, J. Ma, S. Lin, M. Li, Y. Bao, L. Chu, K. Leng, H. Lu, K.P. Loh, A non-dispersion strategy for large-scale production of ultra-high concentration graphene slurries in water, Nat. Commun. 9 (2018) 76, https://doi.org/10.1038/s41467-017-02580-3.
[12] H.C. Schniepp, J.L. Li, M.J. McAllister, H. Sai, M. Herrera-Alonso, D.H. Adamson, R.K. Prud'homme, R. Car, D.A. Saville, I.A. Aksay, Functionalized single graphene sheets derived from splitting graphite oxide, J. Phys. Chem. B 110 (2006) 8535–8539, https://doi.org/10.1021/jp060936f.
[13] P. Vinchon, X. Glad, G. Robert Bigras, R. Martel, L. Stafford, Preferential self-healing at grain boundaries in plasma-treated graphene, Nat. Mater. (2020), https://doi.org/10.1038/s41563-020-0738-0.
[14] O. Balci, N. Kakenov, E. Karademir, S. Balci, S. Cakmakyapan, E.O. Polat, H. Caglayan, E. Özbay, C. Kocabas, Electrically switchable metadevices via graphene, Sci. Adv. 4 (2018) EAAO1749, , https://doi.org/10.1126/sciadv.aao1749.
[15] Y.S. Kim, J.H. Lee, Y.D. Kim, S.-K. Jerng, K. Joo, E. Kim, J. Jung, E. Yoon, Y.D. Park, S. Seoab, S.-H. Chun, Methane as an effective hydrogen source for single-layer graphene synthesis on Cu foil by plasma enhanced chemical vapor deposition, Nanoscale 5 (2013) 1221–1226, https://doi.org/10.1039/C2NR33034B.
[16] T. Yamada, J. Kim, M. Ishihara, M. Hasegawa, Low temperature graphene synthesis using microwave plasma CVD, J. Phys. D. Appl. Phys. 46 (2013) 63001, https://doi.org/10.1088/0022-3727/46/6/063001.
[17] A. Dato, V. Radmilovic, Z. Lee, J. Phillips, M. Frenklach, Substrate-free gas-phase synthesis of graphene sheets, Nano Lett. 8 (2008) 2012–2016, https://doi.org/10.1021/nl8011566.
[18] E. Tatarova, A. Dias, J. Henriques, M. Abrashev, N. Bundaleska, E. Kovacevic, N. Bundaleski, U. Cvelbar, E. Valcheva, B. Arnaudov, A.M. Botelho do Rego, A.M. Ferraria, J. Berndt, E. Felizardo, O.M.N.D. Teodoro, T.H. Strunskus, L.L. Alves, B. Gonçalves, Towards large-scale in freestanding graphene and N-graphene sheets,

Sci. Rep. 7 (2017) 10175, https://doi.org/10.1038/s41598-017-10810-3.
[19] R. Rincón, C. Melero, M. Jiménez, M.D. Calzada, Synthesis of multi-layer graphene and multi-wall carbon nanotubes from direct decomposition of ethanol by microwave plasma without using metal catalysts, Plasma Sources Sci. Technol. 24 (2015) 032005, , https://doi.org/10.1088/0963-0252/24/3/032005.
[20] A. Dato, Graphene synthesized in atmospheric plasmas—a review, J. Mater. Res. 34 (2019) 1–17, https://doi.org/10.1557/jmr.2018.470.
[21] C. Melero, R. Rincón, J. Muñoz, G. Zhang, S. Sun, A. Perez, O. Royuela, C. González-Gago, M.D. Calzada, Scalable graphene production from ethanol decomposition by microwave argon plasma torch, Plasma Phys. Control. Fusion 60 (2018) 014009, , https://doi.org/10.1088/1361-6587/aa8480.
[22] Y. Kabouzi, M. Moisan, J.C. Rostaing, C. Trassy, D. Guerin, D. Keroack, Z. Zakrzewski, Abatement of perfluorinated compounds using microwave plasmas at atmospheric pressure, J. Appl. Phys. 93 (2003) 9483–9496, https://doi.org/10.1063/1.1574595.
[23] A. Dato, Z. Lee, K.-J. Jeon, R. Erni, V. Radmilovic, T.J. Richardsonc, M. Frenklachd, Clean and highly ordered graphene synthesized in the gas phase, Chem. Commun. 6 (2009) 6095–6097 https://doi.org/10.1039/B911395A.
[24] A. Dato, M. Frenklach, Substrate-free microwave synthesis of graphene: experimental conditions and hydrocarbon precursors, New J. Phys. 12 (2010) 125013, https://doi.org/10.1088/1367-2630/12/12/125013.
[25] A. Münzer, L. Xiao, Y.H. Sehlleier, C. Schulz, H. Wiggers, All gas-phase synthesis of graphene: characterization and its utilization for silicon-based lithium-ion batteries, Electrochim. Acta 272 (2018) 52e59, https://doi.org/10.1016/j.electacta.2018.03.137.
[26] E. Tatarova, J. Henriques, C.C. Luhrs, A. Dias, J. Phillips, M.V. Abrashev, C.M. Ferreira, Microwave plasma based single step method for free standing graphene synthesis at atmospheric conditions, Appl. Phys. Lett. 103 (2013) 134101, https://doi.org/10.1063/1.4822178.
[27] E. Tatarova, A. Dias, J. Henriques, A.M. Botelho do Rego, A.M. Ferraria, M.V. Abrashev, C.C. Luhrs, J. Phillips, F.M. Dias, C.M. Ferreira, Microwave plasmas applied for the synthesis of free standing graphene sheets, J. Phys. D 47 (2014) 385501, https://doi.org/10.1088/0022-3727/47/38/385501.
[28] D. Tsyganov, N. Bundaleska, E. Tatarova, A. Dias, J. Henriques, A. Rego, A. Ferraria, M.V. Abrashev, F.M. Dias, C.C. Luhrs, J. Phillips, On the plasma-based growth of 'flowing' graphene sheets at atmospheric pressure conditions, Plasma Sources Sci. Technol. 25 (2016) 015013, , https://doi.org/10.1088/0963-0252/25/1/015013.
[29] M. Moisan, Z. Zakrzewski, J.C. Rostaing, Waveguide-based single and multiple nozzle plasma torches: the TIAGO concept, Plasma Sources Sci. Technol. 10 (2001) 387–394, https://doi.org/10.1088/0963-0252/10/3/301.
[30] R. Rincón, J. Muñoz, M. Sáez, M.D. Calzada, Spectroscopic characterization of atmospheric pressure argon plasmas sustained with the Torche à Injection Axiale sur Guide d'Ondes, Spectrochim. Acta B 81 (2013) 26–35, https://doi.org/10.1016/j.sab.2012.12.006.
[31] R. Rincón, A. Marinas, J. Muñoz, C. Melero, M.D. Calzada, Experimental research on ethanol-chemistry decomposition routes in a microwave plasma torch for hydrogen production, Chem. Eng. J. 284 (2016) 1117–1126, https://doi.org/10.1016/j.cej.2015.09.062.
[32] R. Rincón, M. Jiménez, J. Muñoz, M. Sáez, M.D. Calzada, Hydrogen production from ethanol decomposition by two microwave atmospheric pressure plasma sources: surfatron and TIAGO torch, Plasma Chem. Plasma Process. 34 (2014) 145–157, https://doi.org/10.1007/s11090-013-9502-4.
[33] R. Rincón, A. Marinas, J. Muñoz, M.D. Calzada, Hydrogen production from ethanol decomposition by microwave plasma TIAGO torch, Int. J. Hydrog. Energy 39 (2014) 11441–11453, https://doi.org/10.1016/j.ijhydene.2014.05.128.
[34] M. Jiménez, R. Rincón, A. Marinas, M.D. Calzada, Hydrogen production from ethanol decomposition by a microwave plasma: influence of the plasma gas flow, Int. J. Hydrog. Energy 81 (2013) 26–35, https://doi.org/10.1016/j.ijhydene.2013.05.004.
[35] NIST library from Varian MS Workstation. https://webbook.nist.gov/chemistry/.
[36] M. Moisan, H. Nowakowska, Surface-wave (SW) sustained plasma columns: their contribution to the modeling of RF and microwave discharges with new insight into some of their features. A survey of other types of SW discharges, Plasma Sources Sci. Technol. 27 (2018) 073001, , https://doi.org/10.1088/1361-6595/aac528.
[37] A. Ganash, A. Al-Jabarti Ghaliah, R.M. Altuwirqi, The synthesis of carbon-based nanomaterials by pulsed laser ablation in water, Mater. Res. Express 7 (2020) 015002, , https://doi.org/10.1088/2053-1591/ab572b.
[38] D.D.L. Chung, Review graphite, J. Mater. Sci. 37 (2002) 1475–1489, https://doi.org/10.1023/A:1014915307738.
[39] N. Iwashita, C.R. Park, H. Fujimoto, M. Shiraishi, M. Inagaki, Specification for a standard procedure of X-ray diffraction measurements on carbon materials, Carbon 42 (2004) 701–714, https://doi.org/10.1016/j.carbon.2004.02.008.
[40] I. Childres, L.A. Jauregui, W. Park, H. Cao, Y.P. Chen, Raman Spectroscopy of Graphene and related Materials, New Developments in Photon and Materials Research, 9 Nova Science Publishers, 2013, pp. 403–418.
[41] R. Saito, A. Jorio, A.G. Souza Filho, G. Dresselhaus, M.S. Dresselhaus, M.A. Pimenta, Probing phonon dispersion relations of graphite by double resonance Raman scattering, Phys. Rev. Lett. 88 (2002) 027401, , https://doi.org/10.1103/PhysRevLett.88.027401.
[42] K.N. Kudin, B. Ozbas, H.C. Schniepp, R.K. Prud'homme, I.A. Aksay, R. Car, Raman spectra of graphite oxide and functionalized graphene sheets, Nano Lett. 8 (2007) 36–41, https://doi.org/10.1021/nl071822y.
[43] S. Stankovich, D.A. Dikin, R.D. Piner, K.A. Kohlhaas, A. Kleinhammes, Y. Jia, Y. Wu, S.T. Nguyen, R. Ruoff, Synthesis of graphene-based nanosheets via chemical reduction of exfoliated graphite oxide, Carbon 45 (2007) 1558–1565, https://doi.org/10.1016/j.carbon.2007.02.034.
[44] A. Kumar, A.A. Voevodin, D. Zemlyanov, D.N. Zakharov, T.S. Fisher, Rapid synthesis of few-layer graphene over Cu foil, Carbon 50 (2012) 1546–1553, https://doi.org/10.1016/j.carbon.2011.11.033.
[45] A. Malesevic, R. Vitchev, K. Schouteden, A. Volodin, L. Zhang, G. van Tendeloo, A. Vanhulsel, C. van Haesendonck, Synthesis of few-layer graphene via microwave plasma enhanced chemical vapour deposition, Nanotechnology 19 (2008) 305604, https://doi.org/10.1088/0957-4484/19/30/305604.
[46] Z. Sun, Z. Yan, J. Yao, E. Beitler, Y. Zhu, J.M. Tour, Growth of graphene from solid carbon sources, Nature 468 (2010) 549–552, https://doi.org/10.1038/nature09579.
[47] J. Kim, S.B. Heo, G.H. Gu, J.S. Suh, Fabrication of graphene flakes composed of multi-layer graphene sheets using a thermal plasma jet system, Nanotechnology 21 (2010) 95601, https://doi.org/10.1088/0957-4484/21/9/095601.
[48] M. Passoni, V. Russo, D. Dellasega, F. Causa, F. Ghezzi, D. Wolverson, C.E. Bottani, Raman spectroscopy of non-stacked graphene flakes produced by plasma microjet deposition, J. Raman Spectrosc. 43 (2012) 884–888, https://doi.org/10.1002/jrs.3111.
[49] S. Lee, K. Lee, Z. Zhong, Wafer scale homogeneous bilayer graphene films by chemical vapor deposition, Nano Lett. 10 (2010) 4702–4707, https://doi.org/10.1021/nl1029978.
[50] W. Liu, H. Li, C. Xu, Y. Khatami, K. Banerjee, Synthesis of high-quality monolayer and bilayer graphene on copper using chemical vapor deposition, Carbon 49 (2011) 4122–4130, https://doi.org/10.1016/j.carbon.2011.05.047.
[51] M.P. Lavin-Lopez, J.L. Valverde, M.C. Cuevas, A. Garrido, L. Sanchez-Silva, P. Martinez, A. Romero-Izquierdo, Synthesis and characterization of graphene: influence of synthesis variables, Phys. Chem. Chem. Phys. 16 (2014) 2962–2970, https://doi.org/10.1039/c3cp54832e.
[52] A.C. Ferrari, J.C. Meyer, V. Scardaci, C. Casiraghi, M. Lazzeri, F. Mauri, S. Piscanec, D. Jiang, K.S. Novoselov, S. Roth, A.K. Geim, Raman spectrum of graphene and graphene layers, Phys. Rev. Letter. 97 (2006) 187401, https://doi.org/10.1103/PhysRevLett.97.187401.
[53] N. Larouche, B.L. Stansfield, Classifying nanostructured carbons using graphitic indices derived from Raman spectra, Carbon 48 (2010) 620–629, https://doi.org/10.1016/j.carbon.2009.10.002.
[54] D.S. Knight, W.S. White, Characterization of diamond films by Raman spectroscopy, J. Mater. Res. 4 (1989) 386–393, https://doi.org/10.1557/JMR.1989.0385.
[55] T. Terasawa, K. Saiki, Growth of graphene on Cu by plasma enhanced chemical vapor deposition, Carbon 50 (2012) 869–874, https://doi.org/10.1016/j.carbon.2011.09.047.